Journal of Energy Chemistry 82 (2023) 375–386

Contents lists available at ScienceDirect

Journal of Energy Chemistry

journal homepage: www.elsevier.com/locate/jechem

http://www.journals.elsevier.com/journal-of-energy-chemistry/

Building up a general selection strategy and catalytic performance prediction expressions of heteronuclear double-atom catalysts for N_2 reduction

Yibo Wu [a], Cheng He [a,*], Wenxue Zhang [b,*]

[a] State Key Laboratory for Mechanical Behavior of Materials, School of Materials Science and Engineering, Xi'an Jiaotong University, Xi'an 710049, Shannxi, China
[b] School of Materials Science and Engineering, Chang'an University, Xi'an 710064, Shannxi, China

ARTICLE INFO

Article history:
Received 8 February 2023
Revised 14 March 2023
Accepted 15 March 2023
Available online 30 March 2023

Keywords:
Heteronuclear double-atom catalyst
Nitrogen reduction reaction
Density functional theory
Prediction expression
Selection strategy

ABSTRACT

The severe environmental problems and the demand for energy urgently require electrocatalysis to replace Haber-Bosch for the nitrogen reduction reaction (NRR). The descriptors and important properties of single-atom and homonuclear double-atom catalysts have been preliminarily explored, but the relationship between the inherent properties and catalytic activity of heteronuclear double-atom catalysts with better performance remains unclear. Therefore, it is very significant to explore the prediction expressions of catalytic activity of heteronuclear double-atom catalysts based on their inherent properties and find the rule for selecting catalytic centers. Herein, by summarizing the free energy for the key steps of NRR on 55 catalysts calculated through the first-principle, the expressions of predicting the free energy and the corresponding descriptors are deduced by the machine learning, and the strategy for selecting the appropriate catalytic center is proposed. The selection strategy for the central atom of heteronuclear double-atom catalysts is that the atomic number of central B atom should be between group VB and VIIIB, and the electron difference between central A atom and B atom should be large enough, and the selectivity of NRR or hydrogen evolution reaction (HER) could be calculated through the prediction formula. Moreover, five catalysts are screened to have low limiting potential and excellent selectivity, and are further analyzed by electron transfer. This work explores the relationship between the inherent properties of heteronuclear double-atom catalysts and the catalytic activity, and puts forward the rules for selecting the heteronuclear double-atom catalytic center, which has guiding significance for the experiment.

1. Introduction

Although nitrogen is abundant in the Earth's ecosystem, about half of the nitrogen atoms in the human body come from the Haber-Bosch process [1–4]. However, the production conditions (high temperature and high pressure) required by the Haber-Bosch process of nitrogen reduction reaction (NRR) are very harsh, and the resulting energy consumption (about 2% of global energy) and pollution (a huge amount of CO_2) pose an increasingly serious threat to human survival [5–11]. The electrocatalytic nitrogen reduction method has the advantages of no pollution and low energy consumption, and can safely produce ammonia under environmentally friendly conditions [12–15]. At present, a variety of catalysts have been proposed, including bulk catalysts, single-atom catalysts, homonuclear double-atom catalysts, and heteronuclear double-atom catalysts. Single-atom catalysts have been widely explored for their improved yields compared to bulk catalysts, such as Mo@BN [16], B@g-C_3N_4 [17], W@g-CN [18], V/γ-BN [19], and so on [20–25]. The multiple protonation processes in NRR make it difficult for the single-atom catalyst to improve the yield and Faraday efficiency at the same time, so the double-atom catalysts are proposed to solve this problem. Among them, the first to be explored is the homonuclear double-atom catalysts, namely, Mo_2@g-C_2N [26], B_4C [27], Mn_2@g-C_2N [28], B_2@BP [29], and Fe_2N_4@G [30]. However, the improvement of the catalytic performance of the homonuclear double-atom catalyst is very limited, while the heteronuclear double-atom catalyst is used to further improve the catalytic performance, which is a continuation of the nitrogenase structure. Heteronuclear double-atom synergies can

* Corresponding authors.
E-mail addresses: hecheng@mail.xjtu.edu.cn (C. He), wxzhang@chd.edu.cn (W. Zhang).

https://doi.org/10.1016/j.jechem.2023.03.024

break the activity law of single-atom catalysts to achieve highly efficient NRR, such as M_1M_2@Pc [31], AuNi@N-doped carbon [32], FeRh@NPG [33], VCr@NG [34], M_1M_2@GDY [35], M_1M_2@g-C_3N_4 [36], and so on [37–39].

In the heteronuclear double-atom catalytic system, different atoms in the catalytic center have different properties, which greatly increases the difficulty of accurately designing catalysts for NRR with high catalytic activity and selectivity. Hence, the traditional methods (trial-and-error approaches) of designing and searching for suitable catalysts are expensive and inefficient [40]. In order to reduce the cost of trial and error, many descriptors on catalyst properties and the free energy change (ΔG) for NRR have been explored. Meanwhile, these descriptors can be divided into two types according to the features of the independent variables they originate from: inherent attributes and computational attributes. So far, both the inherent and computational properties of single-atom catalysts and homonuclear double-atom catalysts have been fully studied, as shown in Fig. 1(a). For single-atom catalysts, the features related to computational properties are transferred electrons [41–43], adsorption energy (*N, *N_2, *NNH, *NH_2) [44,45], NN bond length [18,43], and d-band center [46], while the features related to inherent properties mainly include valence electrons [42,43,46–48], electronegativity [42,43,46–48], group number [46], radius [46,48], and electron affinity [48]. For homonuclear double-atom catalysts, the computational features that have a great influence on the catalytic activity are transferred electrons and adsorption energy (*N, *NNH) [31,33], while the inherent features of atoms, such as valence electrons [49], electronegativities [49], and excess electrons [50], also play a large role in the catalytic activity. Moreover, for heteronuclear double-atom catalysts, only the computational features, such as transferred electrons and adsorption energy (*N, *NNH), have been explored [33], and there is little research on the inherent features so far. However, the computational features cannot be directly obtained in the experiment to accurately design the appropriate catalyst, and the inherent features can avoid this problem. Therefore, for heteronuclear double-atom catalysts with excellent nitrogen reduction performance, the descriptors related to inherent features are very meaningful for experimental material selection and screening, which need to be further explored. And black phosphorus is selected as the substrate because of its large surface area, flexibility, high carrier mobility, and good electrical conductivity [51]. Moreover, black phosphorus has folds and abundant active sites, which are conducive to doping metal active central atoms. Black phosphorus with active metal atom doping has been prepared, such as Se@BP [52], Pt@BP, and Pd@BP [53]. Some catalysts based on black phosphorus have also been predicted and proposed, such as B_2@BP and Ru@BP [29,54].

Herein, the free energy changes of key steps of NRR on 55 double-atom structures are calculated to obtain the key properties and corresponding expressions, and five suitable structures (atom combinations = TiV, TiCo, VCr, VCo, and VNi, substrate = black phosphorus) for catalytic nitrogen reduction are obtained by screening. By summarizing and learning the free energy changes of NRR on these structures, the prediction expressions and the rules of selecting atoms are obtained, as shown in Fig. 1(c). For each key step of NRR, a complex and a simple prediction expression are obtained. And the selection of atoms can refer to the following three rules: (1) when selecting central atoms of catalytic center, the atomic number of central B atom (with more electrons) should be between group VB and VIIIB; (2) try to enlarge the electron difference between central A and B atom; (3) test the selectivity through the prediction expression of hydrogen evolution reaction (HER).

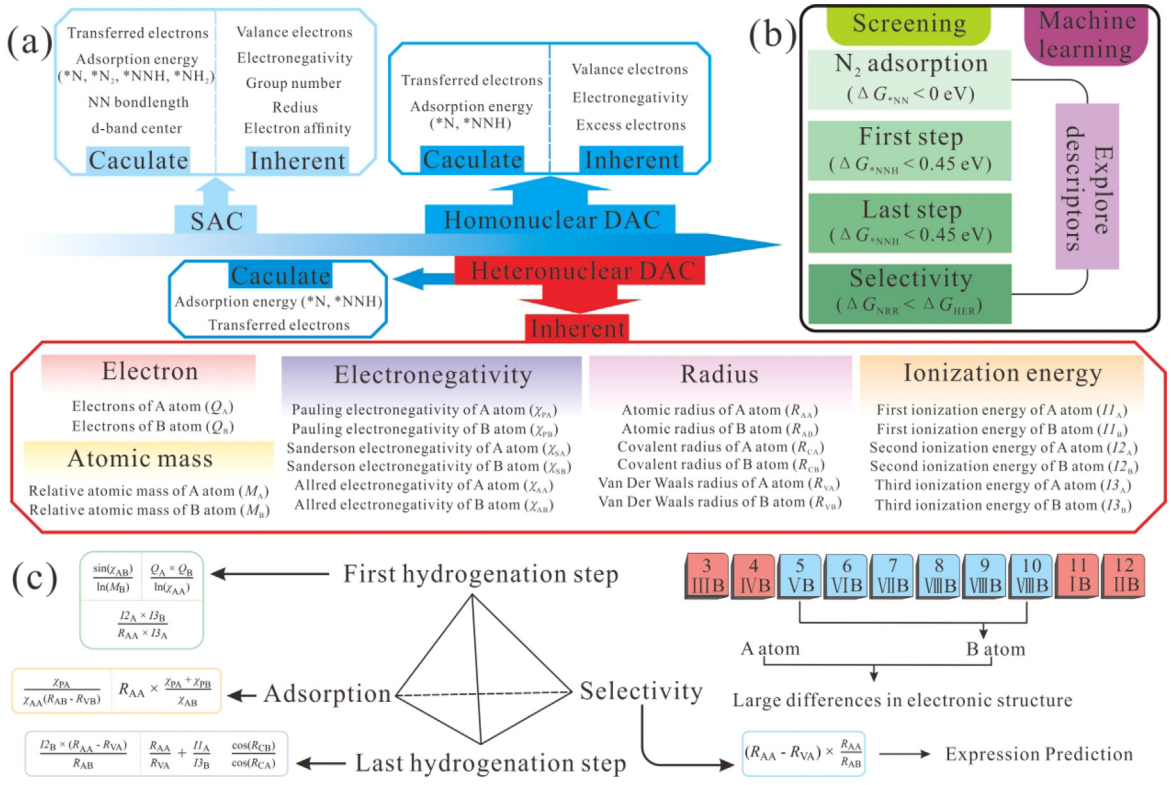

Fig. 1. (a) Development trend of descriptive features in catalysts for NRR. (b) Screening criteria of catalysts for NRR. (c) Descriptors and selection strategies for heteronuclear double-atom catalysts.

2. Theoretical approach

The spin polarization calculation based on the first principle was performed by the Vienna Ab initio Simulation Package (VASP), and the interaction between ions and electrons in the system was described by the projector-augmented wave (PAW) method [55–57]. Perdew, Burke, and Ernzerhof (PBE) functionals in generalized gradient approximation (GGA) were used to deal with exchange–correlation interactions [58]. Cut-off energy of 400 eV was used for structural relaxation, and the Brillouin region was sampled using a 4 × 4 × 1 *k*-point grid of the Monkhorst-pack scheme. The convergence criteria for energy and force are 10^{-5} eV and 0.01 eV/Å, respectively. The interaction of the adsorption interface was treated by the empirical density functional dispersion (DFT-D3) correction [59], and the vacuum space of more than 15 Å in the vertical direction. Binding energy was calculated by the following equation: $E_b = (E_{A\text{-}B@S} - E_S - E_A - E_B)$, where $E_{A\text{-}B@S}$, E_S, E_A, E_B are the energies of doped atoms@substrate, substrate without doped atoms and pristine doped atoms (A, B) respectively. The Gibbs free energy was calculated by the equation [60–62]: $\Delta G = \Delta E + \Delta ZPE - T\Delta S$, where ΔE, ΔZPE, T, and ΔS are the total energy change, zero-point energy change, temperature (T = 298.15 K) and entropy change, respectively. Machine learning (ML) can model from input data by computer algorithms and can be used to describe complex relationships between descriptors and performance [63]. The simple and accurate expressions for predicting the free energy change of important steps in NRR were obtained by using the Sure Independence Screening and Sparsifying Operator (SISSO) package [64–65]. Compared the importance of inherent properties and descriptors using the Random Forest Regressor in scikit-learn. The electron transfer of each part was calculated by Bader analysis.

3. Results and discussion

3.1. Screening and description of ΔG for adsorption

Due to the lack of research on the inherent features of heteronuclear double-atom catalysts, all metal element combinations in the fourth cycle of the periodic table are selected as the catalytic center, with 55 combinations (including 10 homonuclear double-atom catalysts). The binding energy of 55 combinations on black phosphorus is negative, indicating that these structures have thermodynamic stability (Table S1). The screening is carried out from four aspects, namely, (1) the adsorption free energy of nitrogen molecules, (2) ΔG of the first hydrogenation step, (3) ΔG of the last hydrogenation step, and (4) selectivity for NRR, as shown in Fig. 1(b). At the same time, through machine learning, the key properties affecting these steps are analyzed from a bunch of inherent properties (mainly including electron, electronegativity, radius, ionization energy, and atomic mass), and the corresponding descriptors (φ) and expressions are obtained.

The adsorption of nitrogen is decisive for NRR because adsorption is not only the primary condition for NRR, but more importantly, the "contribution and backdonation" mechanism of electrons during the adsorption will promote the subsequent catalytic reaction. At present, there are three main modes to adsorb nitrogen with double-atom catalysts, namely, side-on adsorption, end-on adsorption, and physical adsorption, as shown in Fig. 2 (b). Among them, the first two modes are mainly explored, which is due to the substrate can interact with nitrogen electronically through these two modes. The adsorption free energy is less than 0 eV as the first screening condition, because in this case, the catalytic center can spontaneously capture nitrogen to carry out the next reaction. Fig. 2(a) aggregates the minimum values of adsorption free energy through the end-on and side-on modes. When 13 double-atom combinations (CrCr, CrMn, CrZn, MnMn, MnFe, MnNi, MnCu, FeFe, CoCo, NiCu, NiZn, CuZn, ZnZn) are used as catalytic centers, ΔG of nitrogen adsorption are greater than 0 eV, resulting in they are difficult to capture nitrogen and interact with nitrogen electronically, so they are excluded. Therefore, it is indicated that the larger the number of groups for the element in the periodic table, the more likely the adsorption free energy is greater than 0 eV, because metal atoms with a large number of groups have more valence electrons, and there are almost no empty orbitals to capture the lone pair electrons of nitrogen after binding with the substrate. The side-on adsorption requires both metal atoms as the catalytic center to have appropriate empty orbitals to capture the lone pair electrons of nitrogen, while end-on adsorption mainly requires one of the empty orbitals in the catalytic center, so the end-on adsorption is more convenient to meet the requirements of adsorption free energy. Moreover, the number of catalysts that meet the adsorption free energy requirements in the end-on adsorption is more than that in the side-on adsorption, and almost all catalytic centers that meet the adsorption requirements in the side-on adsorption can also meet the requirements in the end-on adsorption (except NiNi), which is in line with our expectations (Fig. S1). However, the adsorption free energy of end-on adsorption is not necessarily lower than that of side-on adsorption, because when the conditions (both catalytic centers have empty orbitals that capture the lone pair electrons of nitrogen) of side-on adsorption are satisfied, the adsorption free energy of side-on adsorption may be lower than that of end-on adsorption, such as ScCr, VCo, etc.

To further explore the inherent factors affecting nitrogen adsorption, the SISSO method is applied to extract important properties and search for appropriate descriptors. Meanwhile, the importance of each property will be obtained by Random Forest Regressor. The database of inherent properties is mainly the five categories mentioned before, in which electrons are the valence electrons of each catalytic center (Q), atomic mass is the mass of each catalytic center (M), electronegativity includes Pauling electronegativity (χ_P), Sanderson electronegativity (χ_S), and Allred electronegativity (χ_A) of each catalytic center, radius includes atomic radius (R_A), covalent radius (R_C) and van der Waals radius (R_V) of each catalytic center, and ionization energy includes the first ionization energy ($I1$), the second ionization energy ($I2$) and the third ionization energy ($I3$) of each catalytic center. In order to better describe the double-atom catalytic system, we define two atoms in the catalytic center respectively: the central A atom is the one with fewer valence electrons, and the central B atom is the one with more valence electrons. In order to more clearly show the relationship between the inherent properties and the adsorption free energy, the end-on adsorption and side-on adsorption will be considered separately. For side-on adsorption, the most important ten inherent properties are extracted by the SISSO method, and the specific expression is as follows.

$$\Delta G_{**NN} = 181.96 \times \frac{\chi_{PA}}{\chi_{AA}(R_{AB} - R_{VB})} + 0.01854 \times \frac{\cos(R_{AB})}{\sin(R_{VB})} + 0.2874 \times \frac{\cos(\chi_{SA})}{\cos(I3_B)} + 0.2358 \times \sin(Q_B) \times (\chi_{SA} - \chi_{SB}) - 0.1161 \times \cos\left(\frac{I2_A}{M_B}\right) + 2.16 \quad (1)$$

where Q_B, χ_{PA}, χ_{SA}, χ_{SB}, χ_{AA}, R_{AB}, R_{VB}, $I2_A$, $I3_B$, M_B are valence electrons of central B atom, Pauling electronegativity of central A atom, Sanderson electronegativity of central A atom and B atom, Allred electronegativity of central A atom, the atomic radius of central B atom, van der Waals radius of central B atom, the second ionization energy of central A atom, the third ionization energy of central B atom, the relative mass of central B atom, and the following has

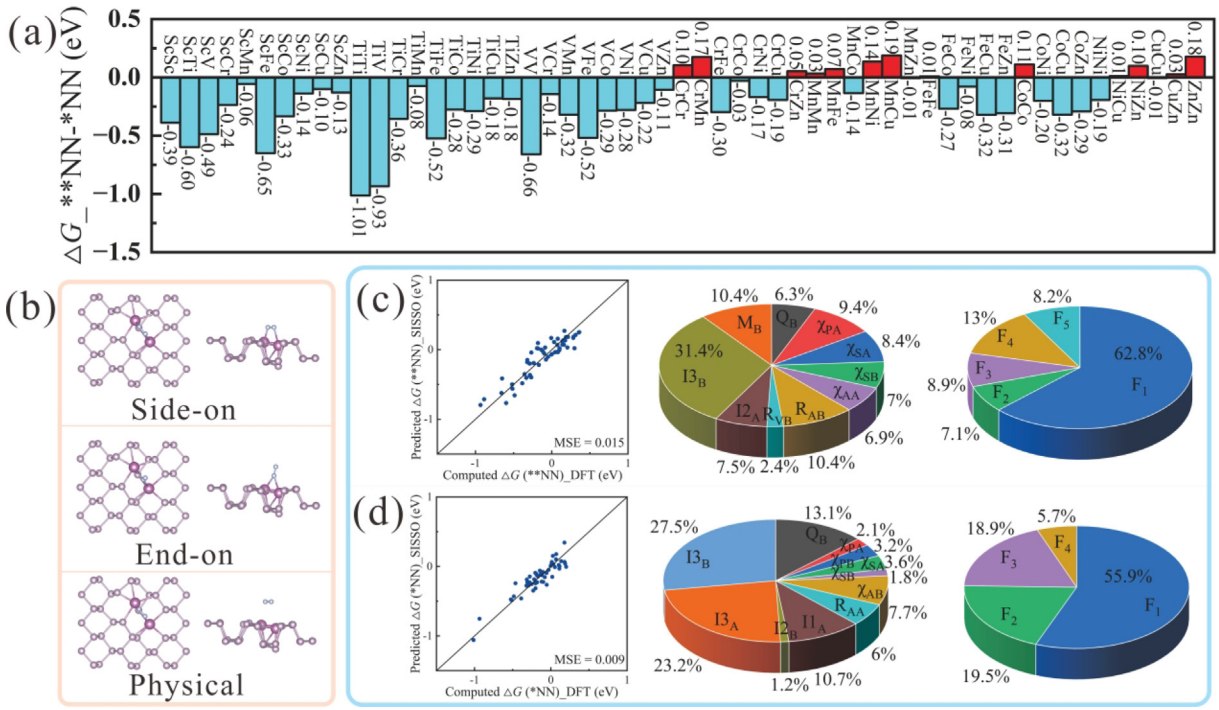

Fig. 2. (a) Nitrogen adsorption free energy of catalysts for NRR. (b) Three adsorption modes of nitrogen. (c) ΔG_{**NN} and (d) ΔG_{*NN} of DFT vs. SISSO predicted, feature importance and factor importance.

the same symbol of the same interpretation will not be repeated. Through the analysis of the importance of each property, the most important property is $I3_B$, the change of which will affect the adsorption free energy, as shown in Fig. 2(c). The first factor has the largest influence, which is 62.8%, so this factor needs to be analyzed emphatically. It can be seen that the larger R_{AB} is, the better the adsorption performance is. Which is mainly due to two aspects of reasons: on the one hand, the larger the atomic radius, the easier it is to interact with nitrogen and form chemical bonds. On the other hand, the smaller the number of electrons in an atom with a larger radius in the same period, the more likely it is that an atom with fewer electrons has an empty *d* orbital to capture the lone pair electrons of nitrogen. And R_{AB} decreases as the atomic number increases. Meanwhile, the adsorption free energy is also related to the electronegativity of the central A atom. Therefore, the choice of central B atom with a smaller atomic number is conducive to the side-on adsorption of nitrogen. The above formula is simplified to get the following formula.

$$\Delta G_{**NN} = 138.997 \times \frac{\chi_{PA}}{\chi_{AA}(R_{AB} - R_{VB})} + 1.647 \quad (2)$$

where χ_{PA}, χ_{AA}, R_{AB}, and R_{VB} have been explained above. The mean square error between the free energy predicted by the above simple formula and the calculated results is 0.047 (Fig. S2). The only factor in the formula is consistent with the first factor in the previous complex formula, indicating that this factor does play a decisive role in the side-on adsorption of nitrogen. Hence, the descriptor for side-on adsorption of nitrogen can be defined as $\varphi_{**NN} = \frac{\chi_{PA}}{\chi_{AA}(R_{AB}-R_{VB})}$.

For end-on adsorption, eleven important inherent properties are selected and expressed in the following equation.

$$\Delta G_{*NN} = 0.00072 \times I3_A \times \frac{\chi_{AB}}{\chi_{PA} + \chi_{PB}} + 0.18 \times |\cos(I1_B) - \sin(I1_A)| - 3.467 \times \frac{e^{-Q_B}}{\sin(R_{AA})} - 0.4386 \times |\frac{\chi_{SA}}{\chi_{SB}} - \frac{I3_A}{I3_B}| - 1.23 \quad (3)$$

where $I1_A$, $I3_A$, R_{AA}, χ_{PB}, χ_{AB}, and $I2_B$ are the first ionization energy, the third ionization energy, and the atomic radius of central A atom, Pauling electronegativity, Allred electronegativity and the second ionization energy of central B atom. The most important properties are $I3_A$ and $I3_B$, which are 23.2% and 27.5%, because they affect whether the catalytic center has empty orbitals, as shown in Fig. 2(d). The importance of the first factor accounted for the largest proportion (55.9%). It can be seen that with the increase of $I3_A$, the adsorption free energy increases, because the larger $I3_A$ is, the more unfavorable it is to lose electrons, so it is difficult to obtain empty orbitals to capture the lone pair electrons of nitrogen. Meanwhile, the less electronegative central B atom is beneficial to reduce the adsorption free energy, because the less electronegative central B atom also easy to forms empty orbitals. For ease of calculation, the formula with only unique factors is as follows.

$$\Delta G_{*NN} = -0.006996 \times R_{AA} \times \frac{\chi_{PA} + \chi_{PB}}{\chi_{AB}} + 2.245 \quad (4)$$

where χ_{PA}, χ_{PB}, χ_{AB}, R_{AA} have been explained above. The mean square error of the predicted result is 0.029. The smaller atomic number (with a large atomic radius) of central A atom is conducive to reducing the adsorption free energy, and the smaller atomic number (with small electronegativity) of central B atom is also conducive to the end-on adsorption of nitrogen. Hence, the descriptor for end-on adsorption of nitrogen can be defined as $\varphi_{*NN} = R_{AA} \times \frac{\chi_{PA}+\chi_{PB}}{\chi_{AB}}$.

3.2. Screening and description of ΔG for the first hydrogenation step

For the first hydrogenation step, there are three cases: in the first case, nitrogen is adsorbed on the catalytic center through side-on adsorption, and then hydrogen is first added to the nitrogen atom on the side of central A atom; in the second case, which is also side-on adsorption, the hydrogen atom is added to the nitrogen atom on the side of central B atom; in the third case, nitrogen

is attached to the catalytic center by end-on adsorption, and the hydrogen atom is added to the side of the unadsorbed nitrogen atom (Fig. 3b). For the first hydrogenation step, the standard line of 0.45 eV is selected, which can well exclude many catalysts with poor performance, and the minimum ΔG of the first hydrogenation step on various catalysts is shown in Fig. 3(a). The advantages of double-atom catalysts are twofold: on the one hand, the two atoms have more electrons, which increases the probability of electrons entering the antibonding orbital of nitrogen; on the other hand, in the case of side-on adsorption, the two atoms pull on nitrogen, both of which are conducive to reducing the strength of N-N triple bond. Therefore, the number of catalysts meeting the standard requirements in the case of side-on adsorption of catalysts (22 kinds) is more than that in the case of end-on adsorption (19 kinds), because the double-atom can pull nitrogen by side-on adsorption.

The first type of hydrogenation is the most likely of the several hydrogenation methods, which is not only because nitrogen can be pulled through the double-atom, but central A atom has fewer electrons, which would leave the nitrogen bonded to central A atom, while the other half-full orbital bonded to the hydrogen. When the catalyst is hydrogenated by the first type, 18 combinations meet the standard, including ScSc, ScTi, ScV, ScCr, ScMn, ScFe, TiTi, TiV, TiMn, VCr, VFe, VNi, CrCr, CrFe, MnMn, MnFe, MnCu, and FeFe, as shown in Fig. S3. Eleven important features are filtered, and the expression is as follows.

$$\Delta G_{**\mathrm{NHN}} = 0.254 \times \frac{I2_\mathrm{A} \times I3_\mathrm{B}}{R_\mathrm{AA} \times I3_\mathrm{A}} + 0.1358 \times \frac{\cos(\chi_\mathrm{PA})}{\cos(M_\mathrm{B})} - 0.1842 \times \sin(Q_\mathrm{B} \times M_\mathrm{A}) + 0.2059 \times \sin(R_\mathrm{CA}) \times \cos(I3_\mathrm{B}) - 0.1434 \times \frac{\ln(\chi_\mathrm{SA})}{\cos(\chi_\mathrm{SB})} - 1.7927 \quad (5)$$

where R_{CA}, M_A are the covalent radius of central A atom, the relative atomic mass of central A atom. The most important property is $I3_B$, which accounts for 23%, because that affects the likelihood of electrons going into the antibonding orbital of nitrogen, as shown in Fig. 3(c). Factor 1 is the most important and will be analyzed in detail next, as shown in Fig. S4. $\frac{I2_A}{R_{AA} \times I3_A}$ is the factor related to central A atom, which mainly includes $I2_A$, $I3_A$, and R_{AA}. In the same period, the general rule that can be drawn about the factor of central A atom is that it increases with the atomic number (except Mn, Co, Zn). Therefore, the smaller atomic number of central A atom is conducive to reducing ΔG of the first type of hydrogenation reaction. In factor 1, only $I3_B$ is associated with central B atom, and the smaller $I3_B$ is, the lower the change in free energy of the first type of hydrogenation reaction will be, because the reduction of $I3_B$ is conducive to filling the antibonding orbitals of nitrogen with electrons. $I3_B$ increases with the increase of atomic number, so a smaller atomic number of central B atom is conducive to reducing ΔG of the first type of hydrogenation step. Simplification leads to formulas that are easy to calculate.

$$\Delta G_{**\mathrm{NHN}} = 0.2219 \times \frac{I2_\mathrm{A} \times I3_\mathrm{B}}{R_\mathrm{AA} \times I3_\mathrm{A}} - 1.605 \quad (6)$$

where R_{AA}, $I2_A$, $I3_A$, and $I3_B$ have been explained above. The mean square error of this simple formula is 0.097, as shown in Fig. S5. The fact that the only factor in the simplified formula is the same as the first factor in the complex formula shows that the factor is indeed very important. Hence, the descriptor for the first type of the first hydrogenation step can be defined as $\varphi_{**\mathrm{NHN}} = \frac{I2_\mathrm{A} \times I3_\mathrm{B}}{R_\mathrm{AA} \times I3_\mathrm{A}}$.

For the second type of hydrogenation reaction, there are 16 combinations through screening criteria, slightly less than the first type of hydrogenation, making up part of the combination that cannot be hydrogenated through the first type of hydrogenation, so that the four combinations (TiCr, VMn, CrMn, CrCo) that cannot pass the first type of hydrogenation can be hydrogenated through the second type of hydrogenation. Twelve important properties are extracted and expressed as follows.

$$\Delta G_{**NNH} = 3.8514 \times \frac{Q_A \times Q_B}{\chi_{SA} \times R_{AB}} - 0.0835 \times \frac{cos(I3_A)}{sin(I1_B)} + 0.0506 \times \frac{sin(I3_B)}{cos(R_{AA})} - 0.7437 \times cos(R_{VA}) \times (\chi_{PA} - \chi_{PB}) - 0.107 \times (cos(Q_A) - sin(R_{AB})) + 0.1985 \times cos(R_{CA}) \times sin(I3_B) - 0.317 \quad (7)$$

where Q_A, R_{VA}, $I1_B$ are valence electrons and the van der Waals radius of central A atom, the first ionization energy of central B atom. Q_B and R_{AB} are the most important properties, accounting for 27.5% and 21.4% respectively (Fig. 3d), because the number of electrons in central B atom determines whether the nitrogen atom bonded to central B atom also has suitable half-filled orbitals to bond to the hydrogen atom. The factor 1 is the most important, which is $\frac{Q_A \times Q_B}{\chi_{SA} \times R_{AB}}$, and the importance ratio is 62.4%. Among them, the property of central B atom is the most important. The decrease of Q_B and the increase of R_{AB} is conducive to the reduction of its free energy, indicating that the decrease of the atomic number of central B atom is conducive to the second type of hydrogenation step. To facilitate the calculation, the simple formula is as follows.

$$\Delta G_{**\mathrm{NNH}} = 0.00604 \times \frac{Q_\mathrm{A} \times Q_\mathrm{B}}{\ln(\chi_\mathrm{AA})} - 0.243 \quad (8)$$

where Q_A, Q_B, and χ_{AA} have been explained above. The mean square error of this formula is 0.092. The simple formula has $Q_A \times Q_B$ in the unique factor as well as in the complex formula. The smaller the number of electrons in central B atom, the more the free energy reduction, which is consistent with the inference of the complex formula. Therefore, the descriptor for the second type of the first hydrogenation step can be defined as $\varphi_{**\mathrm{NNH}} = \frac{Q_\mathrm{A} \times Q_\mathrm{B}}{\ln(\chi_\mathrm{AA})}$.

For the third type of hydrogenation reaction, there are 19 combinations that meet the screening conditions, making up for the deficiencies of 3 combinations that cannot be hydrogenated through side-on adsorption (TiCo, VV, VCo). Seven important features are refined and the corresponding expressions are as follows.

$$\Delta G_{*\mathrm{NNH}} = 0.00002487 \times {Q_\mathrm{B}}^3 \times {\chi_\mathrm{AB}}^6 - 0.2033 \times |\sin(Q_\mathrm{A}) - \sin(R_\mathrm{CB})| + 0.1823 \times \sin\left(\frac{I2_\mathrm{A}}{R_\mathrm{CB}}\right) + 0.1574 \times |\cos(I2_\mathrm{A}) - \sin(R_\mathrm{VB})| - 0.1242 \times \cos(\chi_\mathrm{PA} \times R_\mathrm{VB}) + 0.1829 \quad (9)$$

where R_{CB} is the covalent radius of central B atom. Q_B is the most important property, accounting for 37.5%, as shown in Fig. 3(e). Among all factors, factor 1 accounted for the highest proportion (72.3%). $Q_B^3 \times \chi_{AB}^6$ increases with increasing atomic number, so central B atoms with smaller atomic numbers favor the third type of hydrogenation. The smaller number of electrons in the central B atom is advantageous for nitrogen atom bond to both central A atom and B atom. The smaller electronegativity helps central B atoms lose electrons to fill the antibonding orbitals of nitrogen. In addition, the simplification is summarized as follows.

$$\Delta G_{*NNH} = -68.19 \times \frac{sin(\chi_{AB})}{ln(M_B)} + 17.243 \quad (10)$$

where χ_{AB} and M_B have been explained above. The mean square error is 0.062, indicating that it can be estimated by simple calculation. So the descriptor for the third type of the first hydrogenation step can be defined as $\varphi_{*\mathrm{NNH}} = \frac{\sin(\chi_\mathrm{AB})}{\ln(M_\mathrm{B})}$.

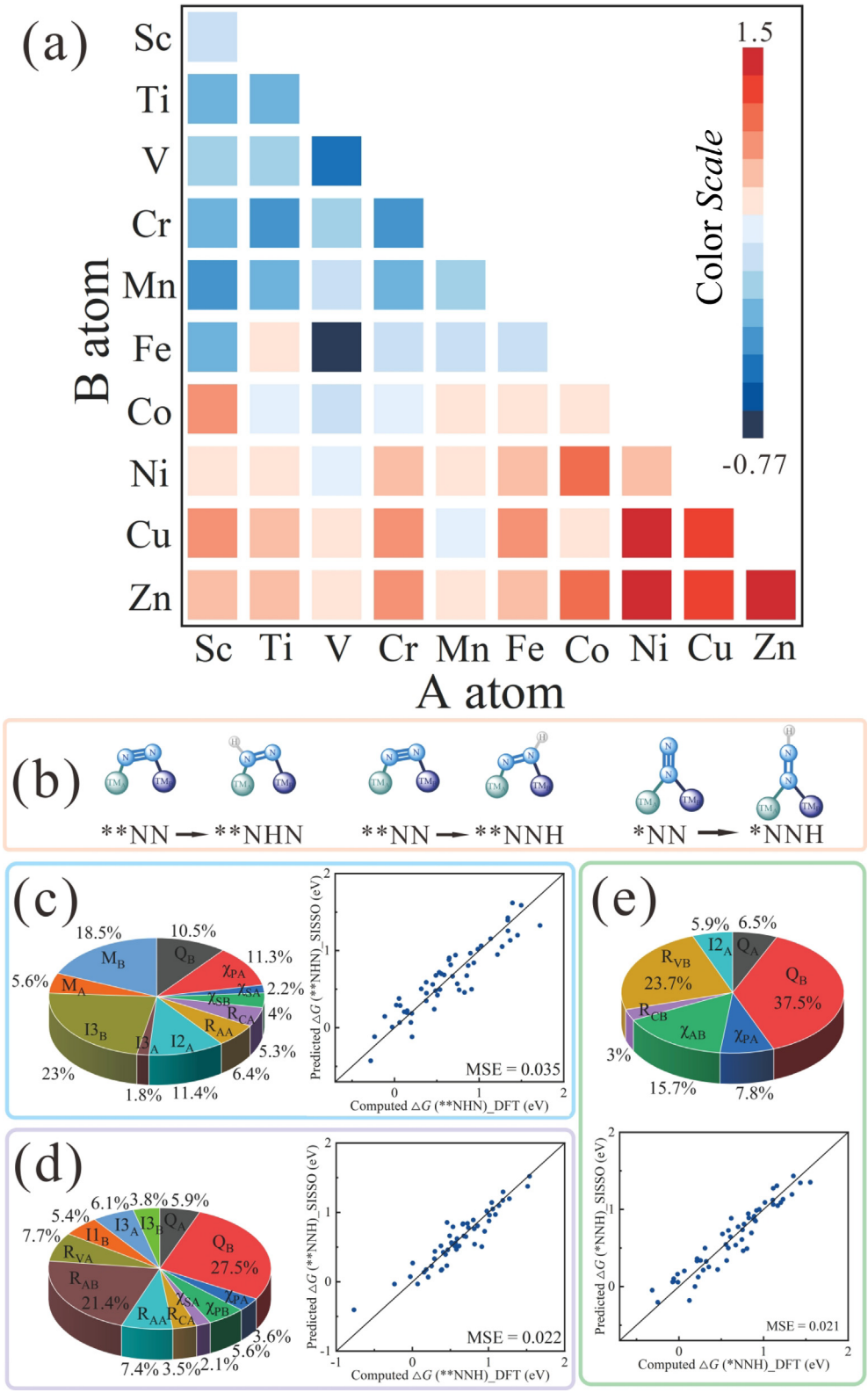

Fig. 3. (a) The free energy changes of the first hydrogenation step in NRR on the catalysts. (b) The first hydrogenation step in three modes. (c–e) The feature importance of three first-step hydrogenation modes, and the calculation and prediction of free energy changes of three first-step hydrogenation modes.

In short, the smaller atomic numbers of central A atom and B atom are conducive to the occurrence of the first hydrogenation step. It can be seen that central B atom with atomic numbers larger than Ni hardly meets the screening of the first hydrogenation step (except MnCu). There are 18 combinations (ScSc, ScTi, ScV, ScCr, ScMn, ScFe, TiTi, TiV, TiMn, VCr, VFe, VNi, CrFe, TiCr, VMn, TiCo, VV, VCo) left after the first and second filters. The reason why CrCo does not meet the conditions is that its adsorption free energy is greater than 0 eV for nitrogen side-on adsorption, and ΔG of the first hydrogenation step is greater than 0.45 eV for nitrogen end-

on adsorption. Therefore, in the selection of catalytic center elements (in the fourth period), elements with atomic numbers less than Cu atoms should be selected as much as possible to increase the possibility of passing the first and second screening steps.

3.3. Screening and description of ΔG for the last hydrogenation step

For the last hydrogenation step, there are two states after hydrogenation: NH_3 group adsorbed on central A atom and B atom respectively (Fig. 4b). Contrary to nitrogen adsorption and the first hydrogenation step, the combination of elements with larger atomic number is beneficial to reduce ΔG of the last hydrogenation step (Fig. 4a).

For the first state of the last hydrogenation step, only ten combinations (ScSc, ScTi, ScV, ScFe, TiTi, TiCr, VV, VCr, VFe, CrFe) fail to meet the screening criteria (Fig. S6). That is because central A is an atom with fewer electrons, which helps the nitrogen in the NH_2 group form coordination bonds with it, so that the nitrogen atom has another half-full orbital to bond with the hydrogen atom. Twelve important features are selected and expressed as follows.

$$\begin{aligned}\Delta G_{*NH_3^1} = {} & 0.003415 \times \frac{I2_B \times (R_{AA} - R_{VA})}{R_{VB}} - 0.0626 \times \frac{\sin(I2_B)}{\cos(R_{CB})} \\ & - 0.00005365 \times Q_A \times \chi_{PB} \times |I3_A - I3_B| \\ & + 0.000843 \times \frac{|R_{CA} - R_{CB}|}{\cos(M_A)} + 0.1018 \times \sin\left(\frac{R_{VA}}{Q_B}\right) \\ & + 2.038 \end{aligned} \quad (11)$$

where R_{CB} is the covalent radius of central B atom. $I2_B$ is the most important property, accounting for 20.2%, as shown in Fig. 4(c). Factor 1 accounts for the largest proportion (75.8%), as shown in Fig. S7. Where the $(R_{AA} - R_{VA})$ is negative because R_{VA} must be greater than R_{AA}. The other term $\frac{I2_B}{R_{VB}}$ is about the property of central B atom, which increases with the increase of the atomic number of central B atom on the whole (except Cr, Zn), so the increase of the atomic number of central B atom is conducive to reducing ΔG of the last hydrogenation step in the first state. At the same time, $|I3_A - I3_B|$ of the factor 3 also indicates that the electron difference between central A and B atoms is also important, and the larger the difference of the third ionization energy between central A and B atom, the more conducive to the occurrence of such hydrogenation steps. It can be seen that this state of hydrogenation reaction cannot occur when central B atom uses an atom whose atomic number is less than V atom, which conforms to the above inference. The simplified formula to facilitate the calculation is as follows.

$$\Delta G_{*NH_3^1} = 0.002194 \times \frac{I2_B \times (R_{AA} - R_{VA})}{R_{AB}} + 1.83 \quad (12)$$

where R_{AA}, R_{AB}, R_{VA}, and $I2_B$ have been explained above. The mean square error is 0.066 (Fig. S8), and the form of the factor is similar to the first factor of the complex formula. Hence, the descriptor for the first state of the last hydrogenation step can be defined as $\varphi_{*NH_3^1} = \frac{I2_B \times (R_{AA} - R_{VA})}{R_{AB}}$.

For the last hydrogenation step in the second state, there are 16 combinations that cannot occur, more than the combinations that cannot occur in the last hydrogenation step in the first state, because central B atom has more electrons than central A atom, and it is more difficult to form a coordination bond with nitrogen atom than central A atom. Although the last hydrogenation step of the second state could not occur in many combinations, the last hydrogenation step of the two combinations (VCr, CrFe) that could not occur in the first state could still be carried out through the second state. Nine important features are selected and expressed as follows.

$$\begin{aligned}\Delta G_{*NH_3^2} = {} & 6.7206 \times \left(\frac{R_{AA}}{R_{VA}} + \frac{I1_A}{I3_B}\right) + 0.0368 \times \frac{\sin(I2_B)}{\sin(I2_A)} \\ & - 0.05425 \times \frac{\sin(M_B)}{\sin(Q_A)} - 0.0805 \times \frac{\sin(I2_A)}{\cos(I3_A)} \\ & - 0.0999 \times (\sin(I3_B) + \sin(M_B)) + 232.844 \\ & \times \frac{\sin(I3_B)}{Q_A^6} - 5.8613 \end{aligned} \quad (13)$$

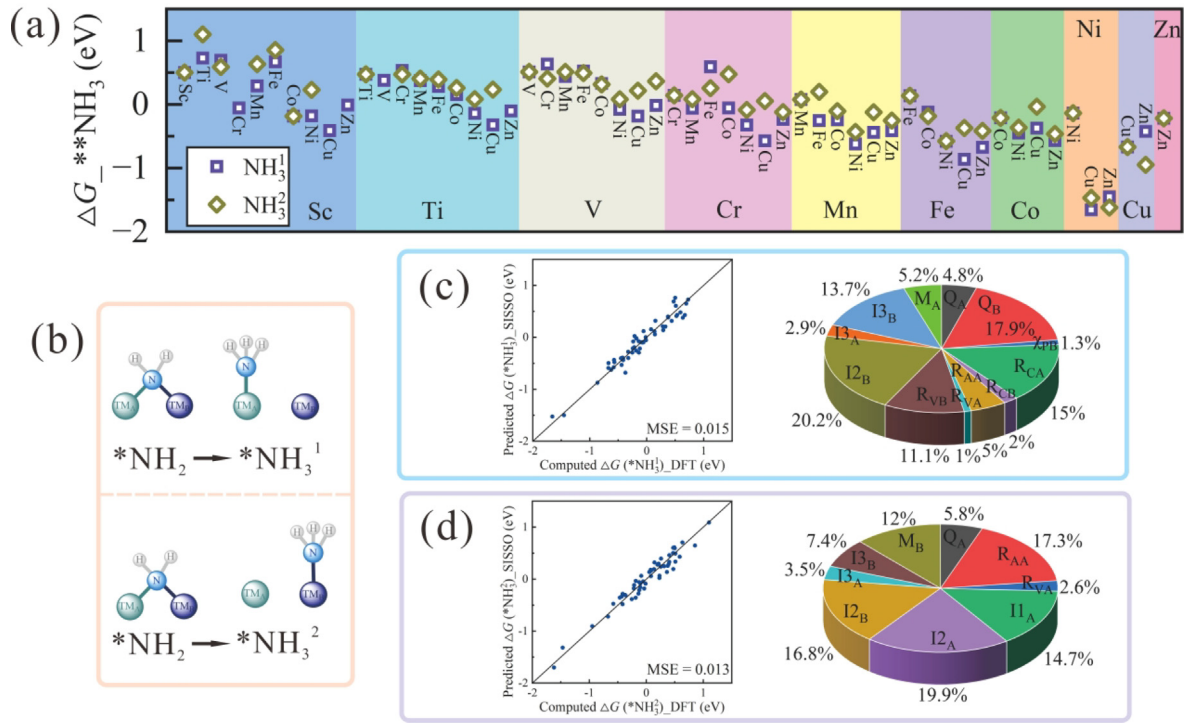

Fig. 4. (a) The free energy changes in two modes of the last hydrogenation step. (b) The last hydrogenation step in two modes. (c and d) The feature importance of two last-step hydrogenation modes, the calculation and prediction of free energy changes.

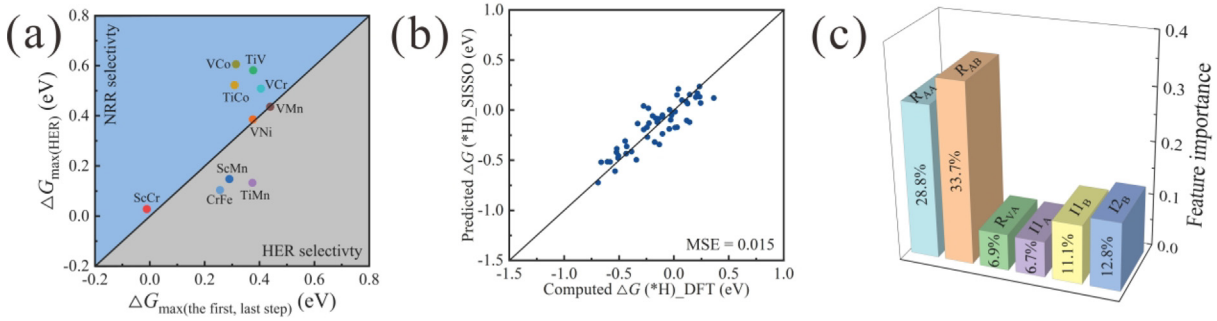

Fig. 5. (a) Free energy changes in HER and the highest free energy changes in the first and last hydrogenation steps of the ten catalysts. (b) ΔG_{*H} of DFT vs. SISSO predicted. (c) The feature importance of HER on catalysts.

where Q_A, R_{AA}, R_{VA}, $I1_A$, $I2_A$, $I2_B$, $I3_A$, $I3_B$, and M_B have been explained above. Among them, the properties of ionization energy (second ionization energy, accounting for 36.7%) and radius are the most important, accounting for 62.3% and 19.9% respectively, as shown in Fig. 4(d). Factor 1 is the most important factor, accounting for 73.5%. There are two main terms for the first factor, $\frac{R_{AA}}{R_{VA}}$ and $\frac{I1_A}{I3_B}$. For the first term $\frac{R_{AA}}{R_{VA}}$, it decreases with the increase of atomic number, so the larger atomic number of central A atom is conducive to reducing ΔG of the last hydrogenation step in the second state. And central A atom is the one that has fewer electrons relative to central B atom, so it's necessary for central B atom to have a larger atomic number. For the second term 2, the decrease of $I1_A$ and the increase of $I3_B$ is conducive to the reduction of free energy, and the values of the first ionization energy and the third ionization energy increase with the increase of atomic number, so the difference in electronic structure of central A and B atoms is conducive to the last hydrogenation step in the second state. It can be seen that when atomic number of central B atom is less than V, reaction cannot occur in this case, which is consistent with the above inference. In addition, the simplification is as follows.

$$\Delta G_{*NH_3^2} = 9.1355 \times \left(\frac{R_{AA}}{R_{VA}} + \frac{I1_A}{I3_B}\right) + 0.0556 \times \frac{\cos(R_{CB})}{\cos(R_{CA})} - 8.0949 \quad (14)$$

where R_{CA}, R_{CB}, R_{AA}, R_{VA}, $I1_A$, and $I3_B$ have been explained above. The mean square error is 0.049, and the first factor of the simplified formula is consistent with the complex formula. Hence, the descriptor for the second state of the last hydrogenation step can be defined as $\varphi_{*NH_3^2} = A \times (\frac{R_{AA}}{R_{VA}} + \frac{I1_A}{I3_B}) + B \times \frac{\cos(R_{CB})}{\cos(R_{CA})}$.

In short, the larger atomic number of central B atom and the larger electron difference between central A atom and B atom are conducive to the occurrence of the last hydrogenation step. After the screening of the last hydrogenation step, 10 combinations (ScCr, ScMn, TiV, TiMn, TiCo, VCr, VMn, VCo, VNi, CrFe) meet the three screening conditions and will proceed to the next screening. Therefore, in order to increase the possibility of the last hydrogenation step, central B atom should choose the atom whose atomic number is greater than or equal to V atom, and try to increase the electron difference between central A atom and B atom.

3.4. Selectivity of the NRR and description of HER

Effective inhibition of hydrogen evolution reaction (HER) by the catalyst is the key to obtain high Faradaic efficiency (FE), so that NH_3 can be produced efficiently. Ten combinations that have passed the previous three steps are selected for this step (selectivity of the NRR). If the minimum potential required by the first and last hydrogenation steps is greater than that required by HER, the catalyst is more inclined to HER; otherwise, the catalyst may undergo NRR. However, even through this screening, all the steps still need to be calculated and discussed. It can be seen that four combinations (ScMn, TiMn, VMn, CrFe) tend to catalyze HER, and the other six combinations (ScCr, TiV, TiCo, VCr, VCo, VNi) may have better selectivity for NRR (Fig. 5a). Six features are selected to describe the free energy changes of HER on each catalyst, and are expressed as follows.

$$\Delta G_{*H} = -0.02685 \times (R_{AA} - R_{VA}) \times \frac{R_{AA}}{R_{AB}} + 0.21497 \times \cos(I1_B) \times \cos(I2_B) - 0.008134 \times \frac{\cos(I1_A)}{\sin(R_{VA})} - 2.4698 \quad (15)$$

where R_{AA}, R_{AB}, R_{VA}, $I1_A$, $I1_B$, and $I2_B$ have been explained above. The mean square error (MSE) is 0.015, as shown in Fig. 5(b). Among them, the most important properties are R_{AA} and R_{AB}, accounting for 28.8% and 33.7%, respectively, as shown in Fig. 5(c). Factor 1 is the most important, accounting for 53.4% (Fig. S9). Due to the particularity of HER (the closer the change of free energy is to 0 eV, the better), it is not easy to qualitatively determine which element has the best or worst performance. Therefore, it is suggested to estimate the free energy change by calculating the above formula. To simplify the calculation, a formula containing only a single factor is obtained, as follows.

$$\Delta G_{*H} = -0.0288 \times (R_{AA} - R_{VA}) \times \frac{R_{AA}}{R_{AB}} - 2.6245 \quad (16)$$

where R_{AA}, R_{AB}, and R_{VA} have been explained above. The mean square error of the results obtained by the above formula is 0.024 (Fig. S10). Through the above formula, the free energy change of HER can be obtained conveniently, quickly and accurately. By choosing nitrogen reduction catalytic materials in this way, some catalysts which are very conducive to HER can be excluded. So the descriptor for HER can be defined as $\varphi_{*H} = (R_{AA} - R_{VA}) \times \frac{R_{AA}}{R_{AB}}$.

3.5. NRR path and electronic properties of heteronuclear double-atom catalysts

All possible steps of the six selected combinations have been calculated, which can be divided into TM_A side, mixed side, TM_B side and distal path according to the hydrogenation sequence (Fig. 6a). Fig. 6(b) summarizes ΔG of the first and last hydrogenation steps of the various catalysts. It can be seen that for catalytic activity, the heteronuclear double-atom catalysts are generally greater than the homonuclear double-atom catalysts, and the homonuclear double-atom catalysts are generally greater than the single-atom catalysts. For the ScCr combination, the reaction tends to be carried out through the Sc side path, and the limiting step appears in the second hydrogenation step (ΔG = 0.08 eV),

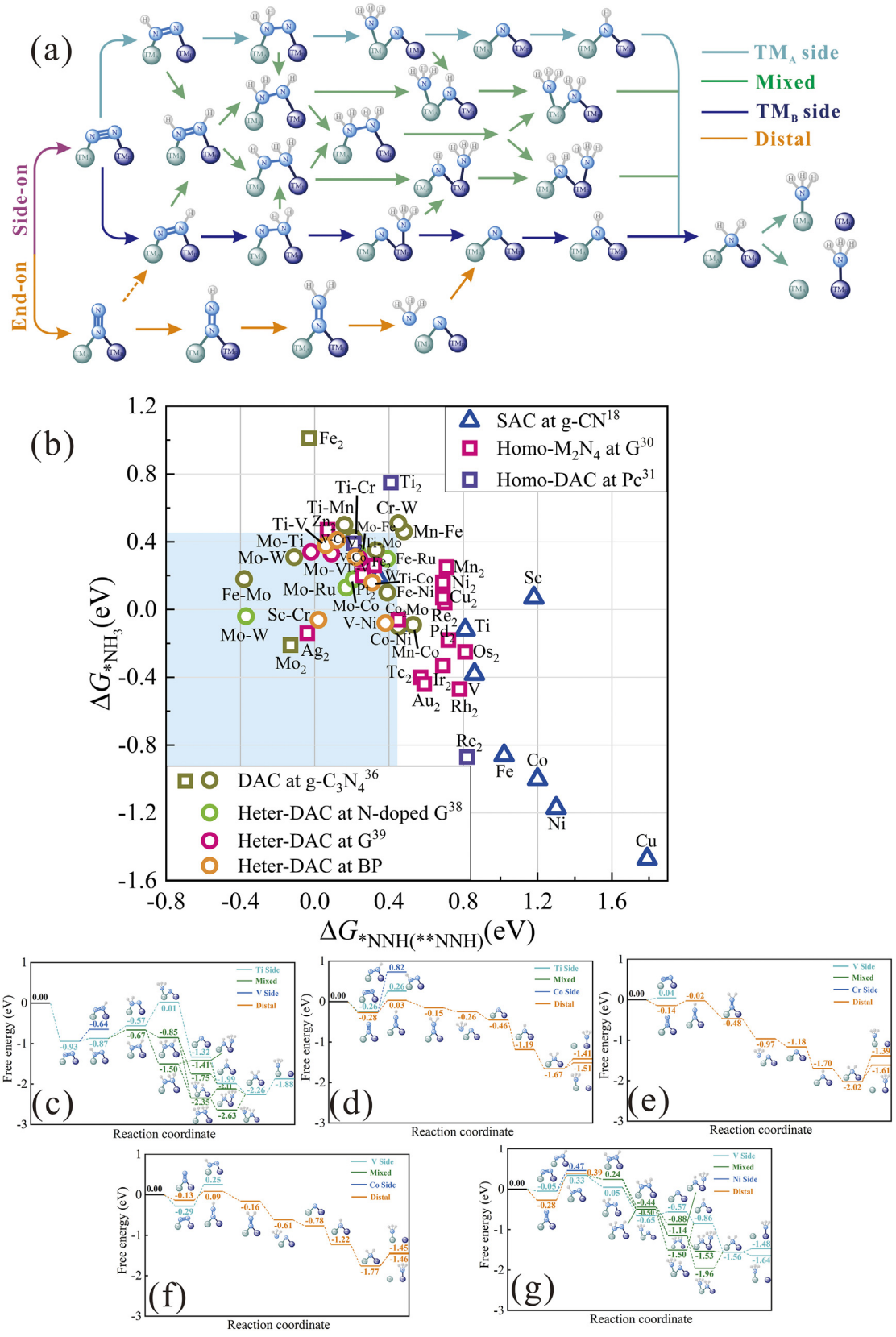

Fig. 6. (a) Schematic for possible mechanisms on heteronuclear double-atom catalysts for NRR. (b) The free energy of the first and last hydrogenation step of different catalysts. Gibbs free energy diagrams for N_2 reduction reaction on (c) TiV@BP, (d) TiCo@BP, (e) VCr@BP, (f) VCo@BP, and (g) VNi@BP, respectively.

mainly because ΔG of the first hydrogenation step (0.02 eV) and the last hydrogenation step (-0.06 eV) is too low (Fig. S11). Although the ScCr combination requires a small voltage to catalyze NRR, it requires a smaller voltage (0.03 V) to catalyze the HER, so the ScCr combination is excluded because of its lack of good selectivity to NRR. For TiV combination, NRR tends to occur through the

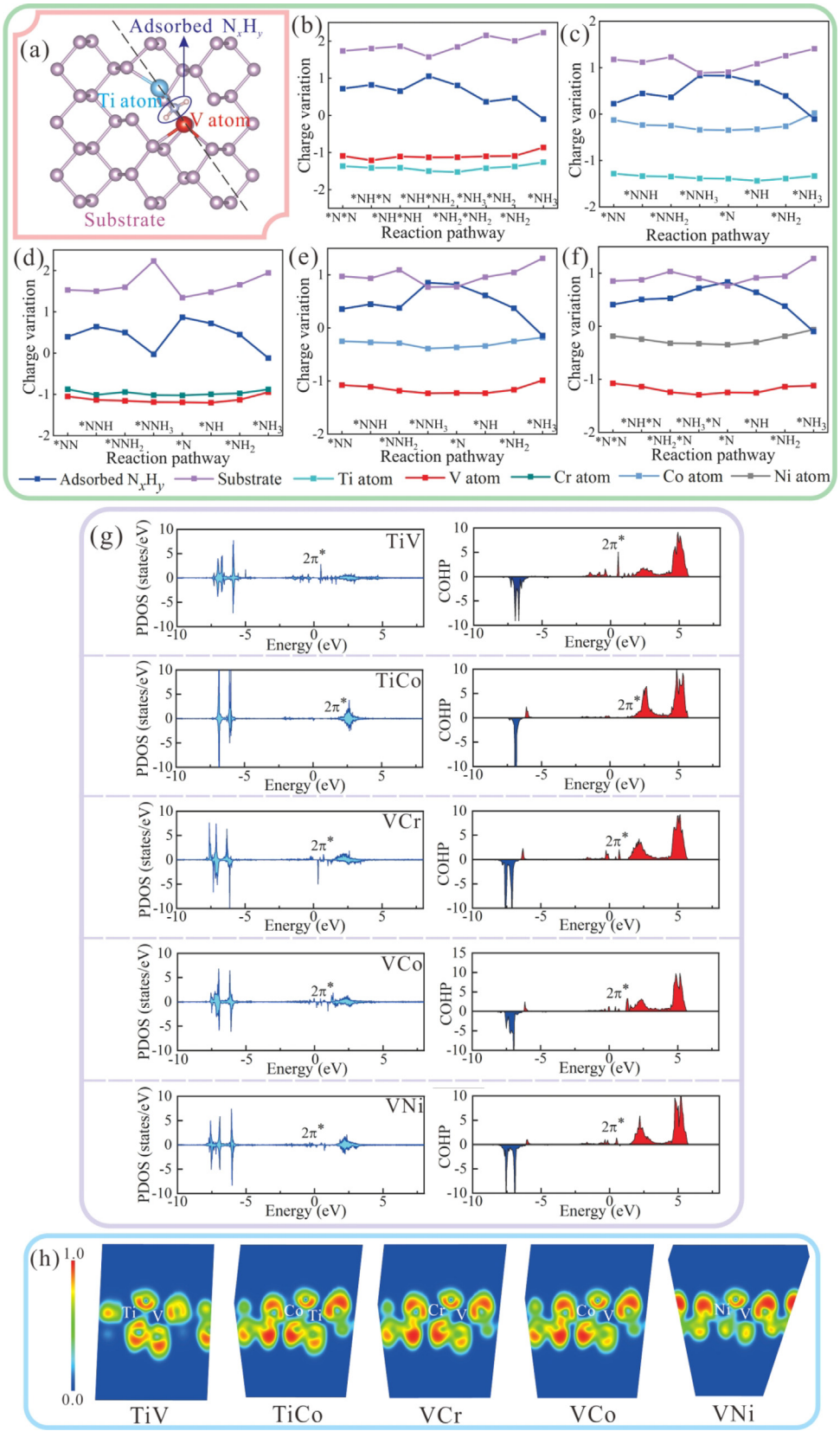

Fig. 7. (a) Schematic diagram of four moieties. Charge fluctuation for the NRR on (b) TiV@BP, (c) TiCo@BP, (d) VCr@BP, (e) VCo@BP, and (f) VNi@BP, respectively. (g) The crystal orbital Hamilton population (COHP) of **NN (*NN) on catalysts. (h) Electron localization function map of $*NH_2$ on catalysts.

mixed path, and the limiting step occurs at the last hydrogenation step, with ΔG of 0.38 eV (Fig. 6c). For TiCo combination, the reaction tends to occur via distal path, and the limiting step occurs at the first hydrogenation step, requiring an external voltage of 0.31 V (Fig. 6d). For both VCr and VCo combinations, NRR tends to be carried out through the distal path, and the limiting step

occurs at the last hydrogenation step, with the free energy increasing by 0.41 eV and 0.31 eV respectively (Fig. 6e and f). For the VNi combination, the reaction tends to be carried out through the V side path, and the limiting step occurs at the first hydrogenation step, with the free energy rising 0.38 eV (Fig. 6g). The specific steps and adsorption structure are shown in Fig. S12. Through the strategy of atom selection and the prediction expression of free energy, the excellent atom combination (YMo) in the fifth period is also predicted. Through the calculation of free energy, the potential determining step is the last hydrogenation step, and the limiting potential is −0.49 V, as shown in Figs. S13 and S14. The charge density difference indicates that the adsorption group has a strong electronic interaction with the catalyst (Fig. S15). And the electron aggregation of nitrogen atoms bonded to central A atom and nitrogen atoms bonded to central B atom is quite different, which is conducive to the occurrence of the first and last hydrogenation steps. In addition, these catalysts could be prepared by the scalable two-step annealing method and atomic layer deposition (ALD). There have been studies on the preparation of heteronuclear double-atom catalysts by the scalable two-step annealing method, such as M_1M_2@NC [66], and some phosphorus-based catalysts have been prepared by ALD, such as Pt@BP and Pd@BP [53].

To further explore the electron transfer in nitrogen reduction process, bader analysis is used to judge the electron gain and loss. The catalyst can be divided into four parts, which are the substrate, N_xH_y group, central A atom and B atom, as shown in Fig. 7(a). The substrate and the N_xH_y group are usually the ones that gain electrons in this process, as shown in Fig. 7(b–f) and Tables S2-S6. Central A atom and B atom are usually the parts that lose electrons, and the number of electrons lost has a great relationship with the atomic properties, such as Ti atom, V atom, Cr atom will lose more electrons, while Co atom and Ni atom lose fewer electrons, which is related to the change of electronegativity, in line with the previous inference. After calculating the density of states and crystal orbital Hamilton population (COHP), it can be seen that the $2\pi^*$ orbital falls near the Fermi level and is easy to be filled by electrons, thus reducing ΔG of the first hydrogenation step (Fig. 7g). The electron localization function (ELF) of the last hydrogenation step is calculated, as shown in Fig. 7(h). It can be concluded that the increase of bonding difference between A-N atoms and B-N atoms is beneficial to reduce ΔG of the last hydrogenation step. For example, TiCo, VCo and VNi have great bonding difference and small free energy change, which are 0.16, 0.31 and −0.08 respectively. The bonding difference between TiV and VCr is small, and the free energy increase is large, which is 0.38 and 0.41 eV, respectively.

4. Conclusions

In conclusion, the complex and simplified formulas for predicting the free energy change of key steps and their corresponding descriptors (nitrogen adsorption: $\varphi^{**}_{NN} = \frac{\chi_{PA}}{\chi_{AA}(R_{AB}-R_{VB})}$ or $\varphi^{*}_{NN} = R_{AA} \times \frac{\chi_{PA}+\chi_{PB}}{\chi_{AB}}$; first hydrogenation step: $\varphi^{**}_{NHN} = \frac{I2_A \times I3_B}{R_{AA} \times I3_A}$ or $\varphi^{**}_{NNH} = \frac{Q_A \times Q_B}{\ln(\chi_{AA})}$ or $\varphi^{*}_{NNH} = \frac{\sin(\chi_{AB})}{\ln(M_B)}$; last hydrogenation step: $\varphi_{*NH_3^1} = \frac{I2_B \times (R_{AA}-R_{VA})}{R_{AB}}$ or $\varphi_{*NH_3^2} = A \times (\frac{R_{AA}}{R_{VA}} + \frac{I1_A}{I3_B}) + B \times \frac{\cos(R_{CB})}{\cos(R_{CA})}$; HER: $\varphi_{*H} = (R_{AA} - R_{VA}) \times \frac{R_{AA}}{R_{AB}}$) for NRR are summarized through 55 double-atom catalysts. Through the analysis of these formulas, the results reveal that for nitrogen adsorption and the first hydrogenation step, the reduction of the atomic number of central B atom is conducive to the reduction of ΔG, and try to make the group number of central B atom less than IB. For the last hydrogenation step, the increase of the atomic number of central B atom is conducive to the reduction of the free energy, and the group number of central B atom should be greater than IVB, and the electron difference between the two atoms should be increased as far as possible. For selectivity, the formula can be used to calculate ΔG of HER directly, and other formulas can be calculated to estimate the major steps of NRR. After calculating and screening the free energy change, five structures are selected to have excellent catalytic activities for NRR, namely TiV, TiCo, VCr, VCo and VNi, with low limiting potential (−0.38, −0.31, −0.41, −0.31, and −0.38 V, respectively) and excellent selectivity for NRR. It is hoped that this work will inspire the development of prediction expressions for heteronuclear double-atom catalytic systems based on inherent atomic properties and have guiding significance for the selection of materials in experiments.

Declaration of competing interest

The authors declare that they have no known competing financial interests or personal relationships that could have appeared to influence the work reported in this paper.

Acknowledgments

The authors acknowledge supports by the National Natural Science Foundation of China (NSFC, 52271113), the Natural Science Foundation of Shaanxi Province, China (2020JM 218), the Fundamental Research Funds for the Central Universities (CHD300102311405), and HPC platform, Xi'an Jiaotong University. We gratefully acknowledge HZWTECH for providing computation facilities.

Appendix A. Supplementary material

Supplementary data to this article can be found online at https://doi.org/10.1016/j.jechem.2023.03.024.

REFERENCES

[1] J.W. Erisman, M.A. Sutton, J. Galloway, Z. Klimont, W. Winiwarter, Nat. Geosci. 1 (2008) 636–639.
[2] J.-G. Chen, R.M. Crooks, L.C. Seefeldt, K.L. Bren, R.M. Bullock, M.Y. Darensbourg, P.L. Holland, B. Hoffman, M.J. Janik, A.K. Jones, M.G. Kanatzidis, P. King, K.M. Lancaster, S.V. Lymar, P. Pfromm, W.F. Schneider, R.R. Schrock, Science 360 (2018) eaar6611.
[3] J. Zhang, X.-Y. Tian, M.-J. Liu, H. Guo, J.-D. Zhou, Q.-Y. Fang, Z. Liu, Q. Wu, J. Lou, J. Am. Chem. Soc. 141 (2019) 19269–19275.
[4] L.-H. Ma, F.-F. Xu, L.-L. Zhang, Z.-F. Nie, K. Xia, M.-X. Guo, M.-Z. Li, X. Ding, J. Energy Chem. 71 (2022) 182–187.
[5] B.H.R. Suryanto, H.-L. Du, D.-B. Wang, J. Chen, A.N. Simonov, D.R. MacFarlane, Nat. Catal. 2 (2019) 290–296.
[6] Y.-L. Wang, W.-J. Yang, S.-S. Xu, S.-F. Zhao, G.-X. Chen, A. Weidenkaff, C. Hardacre, X.-L. Fan, J. Huang, X. Tu, J. Am. Chem. Soc. 144 (2022) 12020–12031.
[7] J.-M. Qi, S.-L. Zhou, K. Xie, S. Lin, J. Energy Chem. 60 (2021) 249–258.
[8] L.-J. Niu, L. An, X.-Y. Wang, Z.-C. Sun, J. Energy Chem. 61 (2021) 304–318.
[9] H.-M. Liu, N. Guijarro, J.-S. Luo, J. Energy Chem. 61 (2021) 149–154.
[10] G.-K. Zheng, L. Li, Z.-Q. Tian, X.-W. Zhang, L. Chen, J. Energy Chem. 54 (2021) 612–619.
[11] X.-T. Li, G.-K. Zhang, P. Shen, X.-L. Zhao, K. Chu, Inorg. Chem. Front. 10 (2022) 280–287.
[12] L. Li, Z. Wu, H. Zhu, G.-H. Robinson, Y. Xie, H.-F. Schaefer, J. Am. Chem. Soc. 142 (2020) 6244–6250.
[13] G. Zhou, T.-H. Li, R. Huang, P.-F. Wang, B. Hu, H. Li, L.-Z. Liu, Y. Sun, J. Am. Chem. Soc. 143 (2021) 5378–5385.
[14] X.-Z. Chen, W.-J. Ong, X.-J. Zhao, P. Zhang, N. Li, J. Energy Chem. 58 (2021) 577–585.
[15] K. Chen, G.-K. Zhang, X.-T. Li, X.-L. Zhao, K. Chu, Nano Res. (2020), https://doi.org/10.1007/s12274-023-5384-9.
[16] J.-X. Zhao, Z.-F. Chen, J. Am. Chem. Soc. 139 (2017) 12480–12487.
[17] C.-Y. Ling, X.-H. Niu, Q. Li, A.-J. Du, J.-L. Wang, J. Am. Chem. Soc. 140 (2018) 14161–14168.
[18] S.-H. Wang, W. Wei, X.-S. Lv, B.-B. Huang, Y. Dai, J. Mater. Chem. A 8 (2020) 1378–1385.
[19] T.-T. Li, Y.-B. Wu, M.-Y. Pei, J. Alloy. Compd. 908 (2022).
[20] J. Li, P. Liu, Y.-Z. Tang, H.-L. Huang, H.-Z. Cui, D.-H. Mei, C.-L. Zhong, ACS Catal. 10 (2020) 2431–2442.
[21] Z. Chen, J.-X. Zhao, C.-R. Cabrera, Z.-F. Chen, Small Methods 3 (2019) 1800368.
[22] X.-M. Yu, P. Han, Z.-X. Wei, L.-S. Huang, Z.-X. Gu, S.-J. Peng, J.-M. Ma, G.-F. Zheng, Joule 2 (2018) 1610–1622.

[23] S. Ji, Z.-X. Wang, J.-X. Zhao, J. Mater. Chem. A 7 (2019) 2392–2399.
[24] J. Wang, Z.-H. Zhang, S.-Y. Qi, Y.-C. Fan, Y.-M. Yang, W.-F. Li, M.-W. Zhao, J. Mater. Chem. A 9 (2021) 19949–19957.
[25] J. Wu, J.-H. Li, Y.-X. Yu, ACS Appl. Mater. Inter. 13 (2021) 10026–10036.
[26] X. Zhang, A. Chen, Z.-H. Zhang, Z. Zhou, J. Mater. Chem. A 6 (2018) 18599–18604.
[27] W.-B. Qiu, X.-Y. Xie, J.-D. Qiu, W.-H. Fang, R.-P. Liang, X. Ren, X.-Q. Ji, G.-W. Cui, A.M. Asiri, G.-L. Cui, B. Tang, X.-P. Sun, Nat. Commun. 9 (2018) 3485.
[28] Z.-W. Chen, J.-M. Yan, Q. Jiang, Small Methods 3 (2019) 1800291.
[29] L. Shi, Q. Li, C.-Y. Ling, Y.-H. Zhang, Y.-X. Ouyang, X.-W. Bai, J.-L. Wang, J. Mater. Chem. A 7 (2019) 4865–4871.
[30] Z. Zhang, X. Huang, H. Xu, ACS Appl. Mater. Inter. 13 (2021) 43632–43640.
[31] X.-Y. Guo, J.-X. Gu, S.-R. Lin, S.-L. Zhang, Z.-F. Chen, S.-P. Huang, J. Am. Chem. Soc. 142 (2020) 5709–5721.
[32] Z.-H. Xue, S.-N. Zhang, Y.-X. Lin, H. Su, G.-Y. Zhai, J.-T. Han, Q.-Y. Yu, X.-H. Li, M. Antonietti, J.-S. Chen, J. Am. Chem. Soc. 141 (2019) 14976–14980.
[33] H.-Y. Li, Z.-F. Zhao, Q.-H. Cai, L.-C. Yin, J.-X. Zhao, J. Mater. Chem. A 8 (2020) 4533–4543.
[34] D.-W. Ma, Y.-Y. Wang, L.-L. Liu, Y. Jia, Phys. Chem. Chem. Phys. 23 (2021) 4018–4029.
[35] D.-W. Ma, Z.-P. Zeng, L.-L. Liu, Y. Jia, J. Energy Chem. 54 (2021) 501–509.
[36] S.-Y. Wang, L. Shi, X.-W. Bai, Q. Li, C.-Y. Ling, J.-L. Wang, ACS Central Sci. 6 (2020) 1762–1771.
[37] Y. Wu, C. He, W. Zhang, J. Am. Chem. Soc. 144 (2022) 9344–9353.
[38] T.-W. He, A.R.P. Santiago, A.-J. Du, J. Catal. 388 (2020) 77–83.
[39] R.-M. Hu, Y.-C. Li, Q.-W. Zeng, F.-H. Wang, J.-X. Shang, Chemsuschem 13 (2020) 3636–3644.
[40] H.-X. Xu, D.-J. Cheng, D.-P. Cao, X.-C. Zeng, Nat. Catal. 1 (2018) 632.
[41] C. Choi, G.-H. Gu, J. Noh, H.S. Park, Y.S. Jung, Nat. Commun. 12 (2021) 4353.
[42] Z.-L. Wen, H.-F. Lv, D.-X. Wu, W.-H. Zhang, X.-J. Wu, J.-L. Yang, J. Phys. Chem. Lett. 13 (2022) 8177–8184.
[43] J. Wang, Z.-H. Zhang, Y.-Y. Li, Y.-Y. Qu, Y.-Q. Li, W.-F. Li, M.-W. Zhao, ACS Appl. Mater. Inter. 14 (2022) 1024–1033.
[44] X.-L. Wang, L.-M. Yang, J. Mater. Chem. A 10 (2022) 1481–1496.
[45] X. Liu, Y. Jiao, Y. Zheng, M. Jaroniec, S.-Z. Qiao, J. Am. Chem. Soc. 141 (2019) 9664–9672.
[46] G.-K. Zheng, Y.-L. Li, X. Qian, G. Yao, Z.-Q. Tian, X.-W. Zhang, L. Chen, ACS Appl. Mater. Inter. 13 (2021) 16336–16344.
[47] Z. Xue, X.-Y. Zhang, J.-Q. Qin, R.-P. Liu, Nano Energy 80 (2021).
[48] W.-H. Zhao, L.-L. Chen, W.-H. Zhang, J.-L. Yang, J. Mater. Chem. A 9 (2021) 6547–6554.
[49] C.-J. Ren, S.-H. Lu, Y.-L. Wu, Y.-X. Ouyang, Y.-H. Zhang, Q. Li, C.-Y. Ling, J.-L. Wang, J. Am. Chem. Soc. 144 (2022) 12874–12883.
[50] X.-S. Lv, W. Wei, B.-B. Huang, Y. Dai, T. Frauenheim, Nano Lett. 21 (2021) 1871–1878.
[51] H.-G. Hu, Z. Shi, K. Khan, R. Cao, W.-Y. Liang, A.K. Tareen, Y. Zhang, W.-C. Huang, Z.-N. Guo, X.-L. Luo, H. Zhang, J. Mater. Chem. A 8 (2020) 5421–5441.
[52] M.-S. Li, W.-H. Li, N. Chen, J.-W. Liang, Y.-Y. Liu, M.-N. Banis, J.-J. Li, Y.-M. Xiao, X.-J. Gao, Y.-F. Hu, Q.-F. Xiao, K. Doyle-Davis, Y.-L. Liu, Y.-M. Yiu, D.-J. Li, S.-Y. Liu, R.-Y. Li, F. Brandys, R. Divigalpitiya, T.K. Sham, X.-L. Sun, Chem. Mater. 33 (2021) 2029–2036.
[53] C. Chen, W. Ou, K.M. Yam, S.-B. Xi, X.-X. Zhao, S. Chen, J. Li, P. Lyu, L. Ma, Y.-H. Du, W. Yu, H.-Y. Fang, C.-H. Yao, X. Hai, H.-M. Xu, M.J. Koh, S.J. Pennycook, J.-L. Lu, M. Lin, C.-L. Su, C. Zhang, J. Lu, Adv. Mater. 33 (2021) 2008471.
[54] J.-.-D. Liu, Z.-X. Wei, Y.-H. Dou, Y.-Z. Feng, J.-M. Ma, Rare Metals 39 (2020) 874–880.
[55] P.E. Blochl, Phys. Rev. B 50 (1994) 17953–17979.
[56] G. Kresse, D. Joubert, Phys. Rev. B 59 (1999) 1758–1775.
[57] G. Kresse, J. Furthmuller, Comp. Mater. Sci. 6 (1996) 15–50.
[58] J.P. Perdew, K. Burke, M. Ernzerhof, Phys. Rev. Lett. 77 (1996) 3865–3868.
[59] L.A. Burns, A. Vazquez-Mayagoitia, B.G. Sumpter, C.D. Sherrill, J. Chem. Phys. 134 (2011).
[60] J.K. Norskov, J. Rossmeisl, A. Logadottir, L. Lindqvist, J.R. Kitchin, T. Bligaard, H. Jonsson, J. Phys. Chem. B 108 (2004) 17886–17892.
[61] J. Rossmeisl, Z.-W. Qu, H. Zhu, G.J. Kroes, J.K. Norskov, J. Electroanal. Chem. 607 (2007) 83–89.
[62] A. Valdes, Z.-W. Qu, G.J. Kroes, J. Rossmeisl, J.K. Norskov, J. Phys. Chem. C 112 (2008) 9872–9879.
[63] S.-R. Lin, H.-X. Xu, Y.-K. Wang, X.-C. Zeng, Z.-F. Chen, J. Mater. Chem. A 8 (2020) 5663–5670.
[64] R.-H. Ouyang, S. Curtarolo, E. Ahmetcik, M. Scheffler, L.M. Ghiringhelli, Phys. Rev. Mater. 2 (2018).
[65] R.H. Ouyang, E. Ahmetcik, C. Carbogno, M. Scheffler, L.M. Ghiringhelli, J. Phys. Mater. 2 (2019).
[66] X. Hai, S.-B. Xi, S. Mitchell, K. Harrath, H.-M. Xu, D.F. Akl, D.-B. Kong, J. Li, Z.-J. Li, T. Sun, H.-M. Yang, Y.-G. Cui, C.-L. Su, X.-X. Zhao, J. Li, J. Perez-Ramirez, J. Lu, Nat. Nanotechnol. 17 (2022) 331.